

On the Influence of Eccentricities on Flux Linkages of Permanent Magnet Synchronous Machines

D. Krahe, J. Kolb and M. Doppelbauer

Abstract—The noise behavior of electrical machines is influenced by tolerances. Eccentricities in particular lead to poorer noise behavior. However, the measurement of NVH quantities is usually very complex. Therefore, it is of interest to be able to detect such tolerances also by other measurands. In this paper, the influence of eccentricities on the flux linkages is investigated. For this purpose, detailed investigations were carried out using FEA. In a further step, these are compared with the results obtained from a test rig measurement. Prior to this, a methodology is presented with which the angle-dependent flux linkages can be determined. It is shown that eccentricities cause only slight changes in the harmonic components of the flux linkages. Due to the symmetry properties of the investigated machine, the changes in the flux linkage caused by the different air gap lengths cancel each other out. This could also be confirmed in the experiment.

Index Terms—dynamic Eccentricity, fault diagnosis, Finite Element Analysis, flux linkage, manufacturing tolerances, Noise Vibration Harshness, Permanent Magnet Synchronous Machine, static Eccentricity

I. INTRODUCTION

In electromobility, operating noise and vibrations still represent a challenge for acoustically responsive mobility solutions that should not be underestimated. The noise is generated by magnetic forces in the machine, which can be divided into radial forces and tangential forces. While the tangential forces generate a usable torque, the radial forces are mainly responsible for the noise behavior of the machine. The radial forces have mode shapes that depend on the design of the machine [1]. If the mode shape and the frequency of the radial force coincide with an inherent shape of the housing, this can lead to undesirable noise. Radial forces and their mode shapes are usually studied in detail during machine design, but idealized models are usually assumed here. Manufacturing and assembly tolerances cause deviations from the ideal shape of the machine, which can be seen, among other things, in eccentricities of the rotor. There are two types of eccentricities, static and dynamic eccentricities. If there is a static eccentricity, the smallest air gap is always located at the same point on the stator. Rotor and rotation axis are therefore equally displaced. In the case of dynamic eccentricity, the narrowest point of the air gap rotates with the speed of the rotor. In this case, the axis of rotation is

still located in the center of the stator bore, while the rotor is displaced with respect to this axis. Both forms of eccentricity result in a changed air gap along the stator circumference. The radial forces depend directly on the air gap length. If this varies, this inevitably leads to a change in the radial forces. In general, further spatial and temporal side orders of the radial forces arise [2]. These side orders can now excite further natural frequencies of the housing, which do not occur in a machine with ideal geometry. This can lead to unexpected noises in real machines, which showed an inconspicuous noise behavior in the design phase. To determine the effects of eccentricities on the vibration behavior, complex Finite Element Analysis (FEA) investigations or Noise Vibration Harshness (NVH) measurements are needed.

Therefore, it is of interest to investigate whether eccentricities also affect electromagnetic quantities such as stator current, induced voltage, and flux linkages. For this purpose, a detailed FEA is performed in this paper. Likewise, the results are compared with real measured data.

II. DETECTING ROTOR ECCENTRICITIES

Some authors have addressed how rotor eccentricities in Permanent Magnet Synchronous Machines (PMSMs) can be detected in the electrical quantities. In [3], Zhu et al. investigated how static and dynamic eccentricities affect the back Electromotive Force (back-EMF). For this purpose, different slot/pole combinations were investigated. It could be shown that for symmetrical machines no significant influence can be detected. Only asymmetrical machines show a measurable influence. Fischer also investigated in [4] the influence of eccentricities on the back-EMF in a machine with parallel coil groups. It could be shown that different back-EMFs occur in the individual coils, but the effect cancels each other out in the whole strand. Furthermore, the effect of eccentricities on the machine currents was investigated in several publications [5]–[7]. For this purpose, the side-band frequencies were analyzed in the power spectral density of the current. However, the measured amplitudes are very small. In [8] it was shown that eccentricities cause zero sequence currents in parallel coil groups. In [9] and [10] eccentricities could be detected by measuring the inductances, but significant differences could only be found in the saturation region.

The effects of eccentricities on the terminal currents and terminal voltages, and thus the flux linkages that can be measured at the terminals, have been little studied. This paper aims to generate further insights into this subject.

D. Krahe and M. Doppelbauer are with the Institute of Electrical Engineering with the Karlsruhe Institute of Technology, 76131 Karlsruhe, Germany (e-mail: dominik.krahe@kit.edu).

J. Kolb is with Schaeffler Technologies AG & Co. KG (SHARE at KIT), 76131 Karlsruhe, Germany

III. THE MACHINE UNDER STUDY

The machine under investigation is a PMSM, which is intended for use in hybrid vehicles. The machine has an maximum output of 80 kW and a maximum speed of 7000 min^{-1} . The winding is a concentrated winding in delta connection. The exact machine parameters can be found in Table I. The winding of the machine has three phases. Each string is divided into eight parallel coil groups.

TABLE I
MAIN PARAMETERS OF THE INVESTIGATED MACHINE

Parameter	Value
max. power	80 kW
max. voltage (DC)	400 V
max. current	420 A _{rms}
max. speed	7000 min^{-1}
max. efficiency (@ 20 °C)	96.2 %
slot number	24
pole-pair number	8
air gap length	1 mm
winding type	concentrated winding
winding connection	Delta connected
slots per pole and phase	$q = 0.5$

A. Static Eccentricity

In the case of static eccentricity, the rotor and the axis of rotation are equally displaced. As a result, all windings along the stator circumference see different air gap lengths. The location of the narrowest air gap remains stationary, i.e. the air gap length is time invariant from the stator's point of view. The largest air gap is exactly opposite, see Fig. 1 (a). Considering the radial forces along the air gap, spatial side orders of harmonics $\nu \pm 1$ arise due to static eccentricities [2]. In the investigated FEA models, a static eccentricity of 0.5 mm in the direction of the x-axis was assumed.

B. Dynamic Eccentricity

Dynamic eccentricity occurs when either the rotor or the axis of rotation is displaced (Fig. 1 (b)). The position of the smallest air gap is variable and rotates with the speed of the rotor. From the stator's point of view, the air gap is time-varying. In the harmonics of the radial forces, this results in temporal and spatial side orders $\nu \pm 1$ [2]. In the investigated FEA models, a dynamic eccentricity of 0.5 mm in x-direction was assumed.

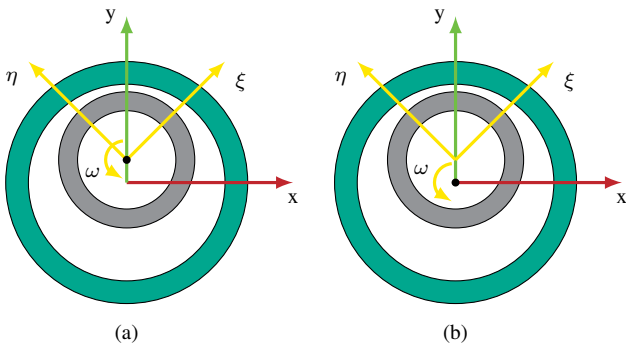


Fig. 1. Static eccentricity (a) and dynamic eccentricity (b)

C. FEA Model

An FEA model of the machine was built for the simulative investigation. Due to the eccentricities, the machine was modeled as a full model. The machine is delta connected. An ideal sinusoidal current is injected into the windings.

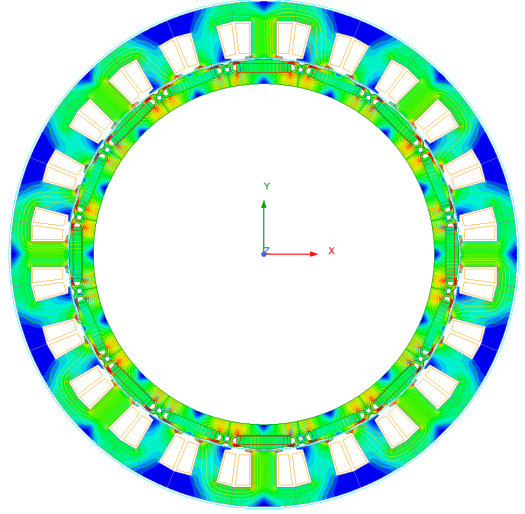


Fig. 2. FEA model of the investigated machine

IV. ANALYSIS OF THE ECCENTRICITIES WITH FEA

In this chapter the results from the FEA simulation are presented. For this purpose, the flux linkages are transformed into the rotor fixed coordinate system (d/q) and decomposed into their frequency components by means of Fourier transformation. The results for the static and dynamic eccentricity are compared with the healthy machine. First, the non-loaded machine is considered. In a second step, the machine is examined under load.

The noise behavior of a PMSM can depend on various factors. The radial forces have an important influence. These radial forces are affected by eccentricities, which generally worsen the noise behavior of the machine [2]. It is to be investigated whether changes occur in the flux linkages and the radial forces in the same way due to tolerances. For this purpose, the changes in the radial forces caused by eccentricities are considered here first. With the simplifying assumption that the magnetic conductivity of the electrical steel is very high and that of the air is very low, the following relationship can be derived using Maxwell's stress tensor [11]:

$$\sigma_{rad} = \frac{B_{rad}^2}{2\mu_0} \quad (1)$$

Where σ_{rad} , B_{rad} and μ_0 are the radial force density, the radial magnetic flux density in the air gap and the vacuum permeability.

Fig. 3 shows the radial force density along the stator circumference at time $t = 0$ s for a healthy machine. Here, the machine is loaded with $I_d = -100$ A and $I_q = 500$ A. It can be seen that the peaks all have the same amplitude.

Fig. 4 shows the curve of the radial force density for a

machine with static eccentricity. For static eccentricity, the maxima are always in the region of the narrowest air gap and do not change with rotor position.

With dynamic eccentricity, the distribution of the radial force density also depends on the rotor position. As can be seen in Fig. 5, the maxima move with the rotation of the rotor.

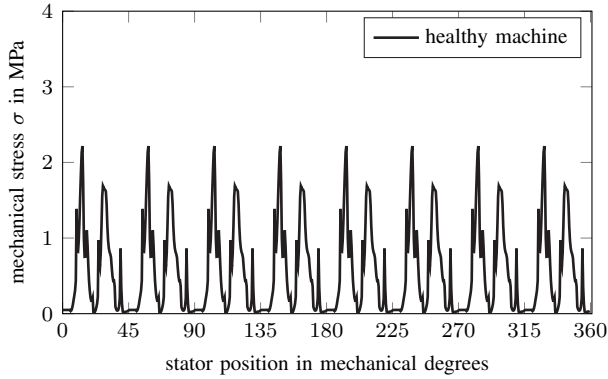


Fig. 3. Maxwell stresses in the airgap at 0° rotor position for the healthy machine under load condition

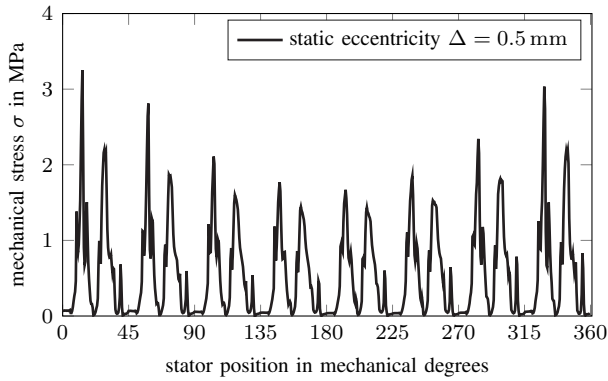


Fig. 4. Maxwell stresses in the airgap at 0° rotor position for the machine with static eccentricity under load condition

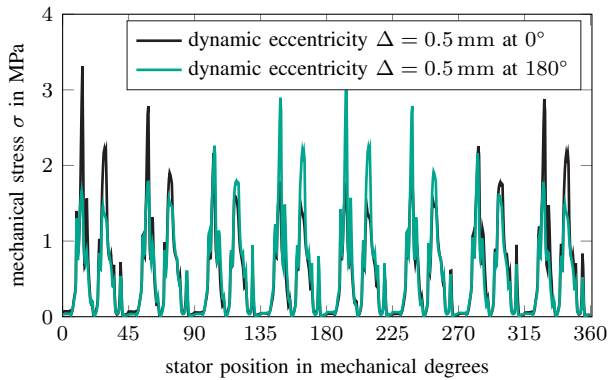


Fig. 5. Maxwell stresses in the airgap at 0° and 180° rotor position for the machine with dynamic eccentricity under load condition

A. Effect of Eccentricities with non-loaded Machine

Figs. 6 and 7 show the harmonics of the flux linkages of the d and q axes for the non-loaded machine ($I_d = I_q = 0$ A). Here, the 0th order represents the fundamental wave

component of the flux linkage. The most prominent orders are multiples of six ($\nu = 6k$, $k \in \mathbb{N}$) [12]. The less pronounced side orders $\nu = 2, 4$ and their harmonics result from the zero sequence currents caused by the delta connection. These zero sequence currents lead to a third order in the stator-fixed x,y,z system, which are modulated accordingly by the d/q-transformation.

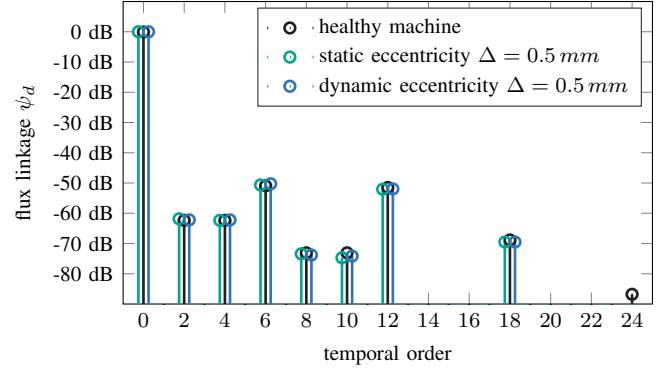


Fig. 6. Harmonic content of d-axis flux linkage under non-load condition

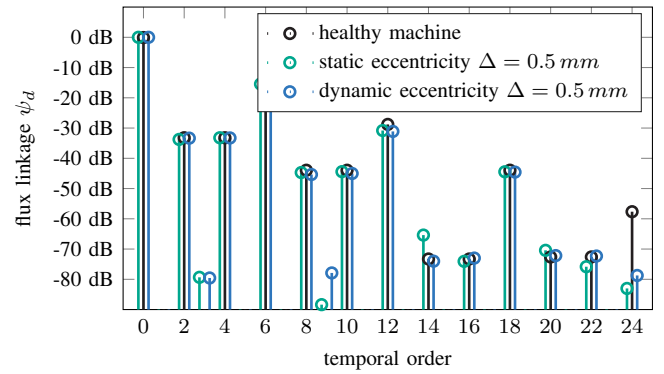


Fig. 7. Harmonic content of q-axis flux linkage under non-load condition

Looking at the harmonic components of the d-flux in Fig. 6, no significant differences can be observed between the healthy machine and the tolerance affected machine. The deviations for both static and dynamic eccentricity are minimal. The same can be seen when considering the flux linkages in the q-direction (Fig. 7). Although the overall harmonic content is greater, the differences between the healthy machine and the eccentricity-affected machine are also very small here. Only the 3rd and 9th order are more prominent. However, in the range of -80 dB, which is too small for a clear detection. Thus, the effects on the radial force densities shown previously are not equally reflected in the flux linkages

B. Effect of Eccentricities with loaded Machine

To investigate the machine under load, a current of $I_d = -100$ A and $I_q = 500$ A was injected into the stator winding of the machine. This corresponds to an operating point near to the characteristic Maximum Torque Per Ampere (MPTA) curve. The results for this are shown in Figs. 8 and 9.

It can be seen here that neither static nor dynamic eccentricity lead to significant deviations from the result of the healthy machine. Based on the results from the investigation of the air gap forces, it could be assumed that the eccentricities also lead to further side orders of $\nu \pm 1$ in the flux linkages. However, this is not observed here. Only in the 18th order a reduction of the amplitude can be seen. The same can be seen when looking at the flux linkages in the q-direction (Fig. 9). Here, in addition to the difference in the 18th order, a small difference in the 12th order with a similar tendency can be seen. Here, too, there is no similar influence as in the case of the radial force density.

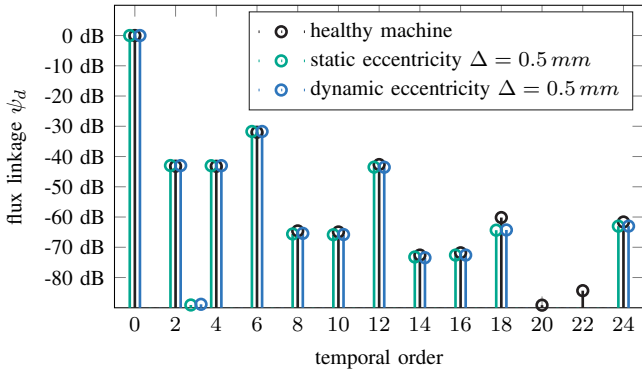


Fig. 8. Harmonic content of d-axis flux linkage under load condition

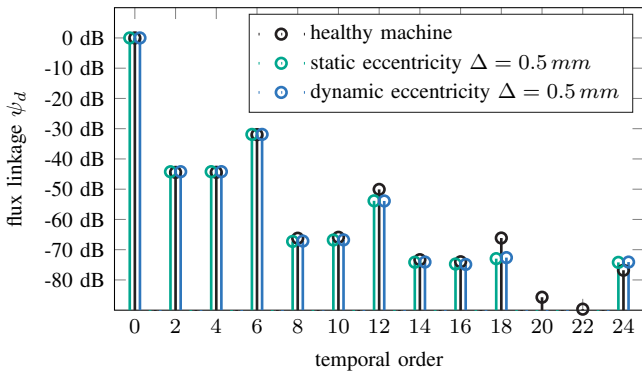


Fig. 9. Harmonic content of q-axis flux linkage under load condition

In order to check whether the phase angle of the harmonics is influenced by the eccentricities, this was also examined.

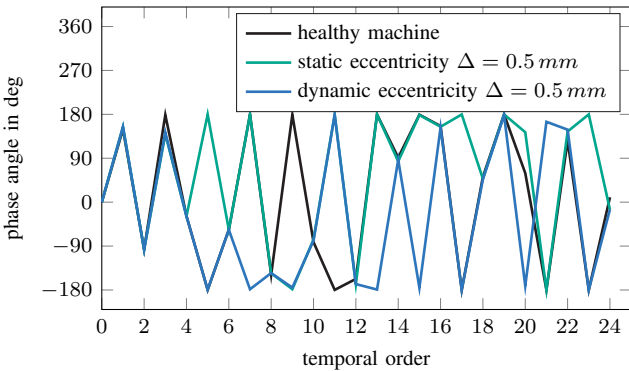


Fig. 10. Phase angle of d-axis flux linkage under load condition

The comparison between healthy machine and machine with eccentricity is shown in Figs. 10 and 11. It can be seen that for all the orders that actually occur, i.e. the even orders, the phase positions match exactly for all three machines.

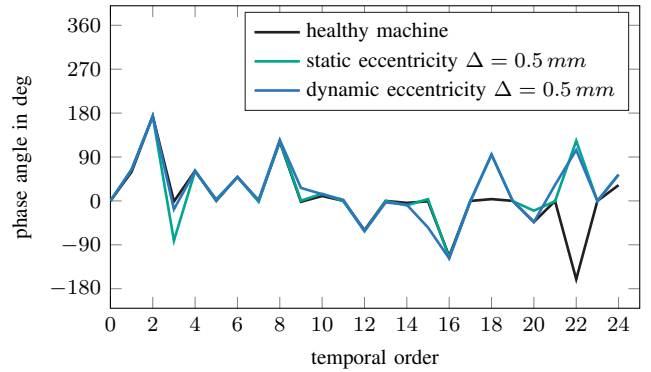


Fig. 11. Phase angle of q-axis flux linkage under load condition

C. Conclusions

The FEA investigations have shown that eccentricities have only a minor influence on the flux linkages. Since in the air gap forces, the eccentricities give rise to side orders with orders $\nu \pm 1$, it had been assumed that similar effects would also be seen in the flux linkages. However, this could not be observed. Thus, in the unloaded machine, the flux linkages for both machines are nearly identical. Looking at the loaded machine, small differences can be seen in the 18th order and also in the 12th order. These differences are in a range > -60 dB, so in principle they should be detectable in a real measurement. Why the differences in the flux linkages turn out to be very small compared to the differences in the air gap forces, however, can be explained as follows. The coils of a string are symmetrically distributed around the circumference of the machine. The coil facing the smallest air gap sees the largest induced voltage. However, because of the symmetry properties of the machine, there is also always a coil on the opposite side at the location of the largest air gap. Due to the parallel connection of the coils in a string, this results in an average induced voltage that corresponds to the voltage of a healthy machine. The same applies to the amplitudes of the harmonics of the flux. Since only even orders occur here, these also cancel each other out by opposing coils. This behavior holds for all symmetric, i.e. machines without unbalanced magnetic pull, and thus explains why the eccentricities have no effect on the flux linkages measured at the terminals [3].

Studies such as by Fischer et al. have shown that when the individual coil groups are considered as open-circuit, there are differences in the back-EMF and thus in the flux linkages for machines with eccentricities. In the case of connected coil groups, eccentricities generate circulating currents which, however, compensate for the effects of the eccentricities, which is why no influence due to eccentricities can be detected at the machine terminals [4].

V. EXPERIMENTAL STUDY

In this chapter, the results from FEA are to be validated with test rig measurements. For this purpose, a method for calculating the angle-dependent flux linkages is first presented.

A. Measurement of the angle-dependent flux linkages

On the test bench, the flux linkages cannot be measured directly, but must be calculated accordingly via the terminal voltages and currents. In order to determine the harmonics of the flux linkages experimentally, however, the flux linkages must be calculated rotor angle-dependent, i.e. all time-dependent quantities in the voltage equations of the machine must be considered. The voltage equations of the machine can generally be described by:

$$u_d = R \cdot i_d + \frac{\partial \psi_d}{\partial i_d} \frac{di_d}{dt} + \frac{\partial \psi_d}{\partial i_q} \frac{di_q}{dt} + \frac{\partial \psi_d}{\partial \gamma} \frac{d\gamma}{dt} - \omega \psi_q \quad (2)$$

$$u_q = R \cdot i_q + \frac{\partial \psi_q}{\partial i_d} \frac{di_d}{dt} + \frac{\partial \psi_q}{\partial i_q} \frac{di_q}{dt} + \frac{\partial \psi_q}{\partial \gamma} \frac{d\gamma}{dt} + \omega \psi_d \quad (3)$$

Where $u_{d,q}$ are the measured terminal voltages, $i_{d,q}$ are the string currents, $\psi_{d,q}$ are the flux linkages, R_S is the stator resistance, ω is the electrical angular frequency and γ is the angular rotor position in electrical degrees. All quantities are considered in the d/q-system. If only fundamental wave maps of the flux linkages are of interest, they can simply be averaged over an electrical period. This eliminates the time derivatives and the equations are easily solved. However, to determine the harmonics, these must also be considered. Thus, the flux linkages depend on the time derivatives of the currents i_d , i_q and the rotor position angle γ . Even if the d/q quantities are assumed to be DC quantities in the model, they exhibit harmonics in reality, which is why the time derivatives are not omitted. This current harmonics are caused by inverter switching, inverter nonlinearities and spatial harmonics of the machine [13]. The equations are a coupled, nonlinear differential equation system, which cannot be solved trivially.

In order to simplify the equations, a so-called repetitive controller is used for the test bench measurements. Such a control scheme is described by Richter [13]. This controller is based on the fact that current harmonics have a repetitive nature during stationary operation. Consequently, a straight forward approach is to identify the effects in one electrical period and feed-forward them in the next period. This simple principle is based on self-learning algorithms and is called repetitive control. Fig. 12 shows the scheme of the control. A conventional current control structure is used as the basis. The currents i_x are measured and closed loop controlled to the reference values i_x^* . The additional scheme drawn in blue extends the current controller with the repetitive control approach. In the identification block the voltage errors Δu_x are calculated. For this purpose, the difference between the actual current i_x and the set current i_x^* is calculated in a first

step. In the next step, the voltage error can be calculated with the help of the rotor speed ω and the flux linkages ψ_x stored in the machine model at the corresponding operating point. This voltage error Δu_x is then stored in the memory block over the rotor angle γ . In the next electrical period, the voltage error at the actual rotor angle can now be read out directly and added to the voltages set by the current controller. This is an iterative approach that requires a few periods until it delivers good results.

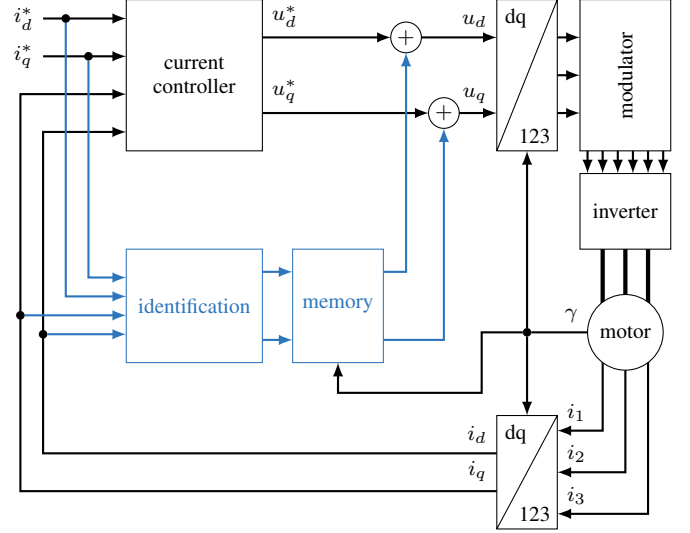


Fig. 12. Scheme of the used control. The repetitive controller is drawn in blue

With the help of this control algorithm, it is possible to achieve approximately constant d/q currents, whereby the time derivatives of the currents can be deleted from the voltage equations. The following simplified equations are now obtained:

$$u_d = R \cdot i_d + \frac{\partial \psi_d}{\partial \gamma} \frac{d\gamma}{dt} - \omega \psi_q \quad (4)$$

$$u_q = R \cdot i_q + \frac{\partial \psi_q}{\partial \gamma} \frac{d\gamma}{dt} + \omega \psi_d \quad (5)$$

This simplifies the equations considerably, but it is still a coupled differential equation. However, if this equation is considered in stator fixed coordinate system (α/β), the following equations are obtained by omitting the rotatory components:

$$u_\alpha = R \cdot i_\alpha + \frac{\partial \psi_\alpha}{\partial \gamma} \frac{d\gamma}{dt} \quad (6)$$

$$u_\beta = R \cdot i_\beta + \frac{\partial \psi_\beta}{\partial \gamma} \frac{d\gamma}{dt} \quad (7)$$

From these equations, the time-dependent flux linkages can now be easily determined by integration:

$$\psi_{\alpha,\beta} = \int u_{\alpha,\beta} - R \cdot i_{\alpha,\beta} dt + c \quad (8)$$

For this, the integration constant c must still be determined. Since the flux linkages must be average-free for an electrical period, this is easy to determine. In a last step, the flux linkages can be transformed into the d/q system with the help of the rotor angle γ .

B. Test Bench Setup

The test stand consists of a load machine and the Device Under Test (DUT) described in section III. Both machines are coupled to each other via a torque measuring shaft. The line voltages, the phase currents and the rotor position angle are recorded. Prior to this, the stator resistance was determined using a milliohm meter. From these quantities, the angle-dependent flux maps can be determined using the method described in Section A. above. An operating point of $I_d = -100$ A and $I_q = 500$ A was set. This is a point close to the characteristic MPTA curve. The measurements were all performed at a speed of $n = 625 \text{ min}^{-1}$. Two different machines are considered for validation:

- Healthy machine without noticeable eccentricity
- Machine with a static eccentricity of $\Delta = 0.3 \text{ mm}$

The machines were taken from series production and measured accordingly. The examined machine has the eccentricity due to manufacturing tolerance and was noise conspicuous in a previous NVH measurement.

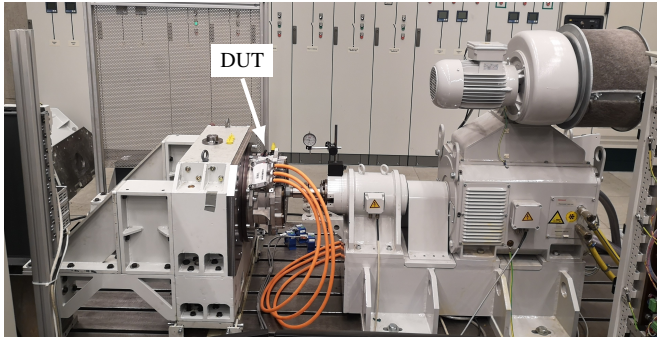


Fig. 13. Test Bench Setup

C. Measurement results

Figs. 14 and 15 show the flux linkage curves over the electrical angle for the selected operating point.

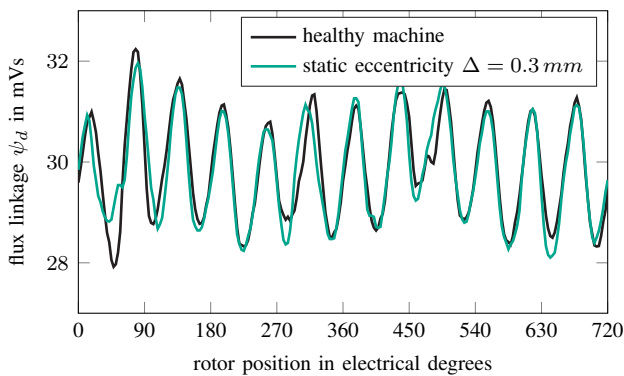


Fig. 14. d-axis flux linkage under load condition

It can be seen that the progressions of the flux linkages coincide well in both axis directions, d- and q-direction. No clear difference due to the eccentricity can be determined.

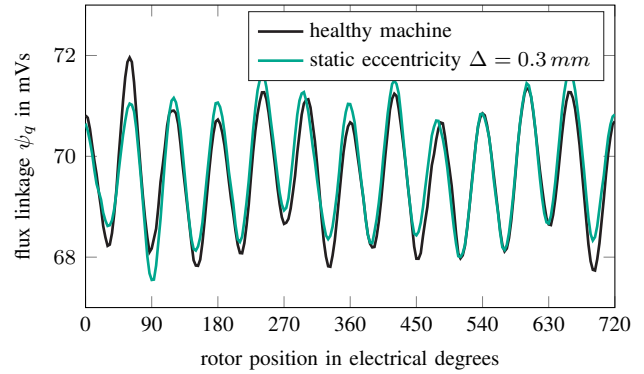


Fig. 15. q-axis flux linkage under load condition

For a closer look, the Fourier transforms of the time signals are shown in Figs. 16 and 17. As already shown in the FEA, a decrease in the 18th order can be seen for the eccentric machine. Likewise, deviations in the 2nd and 4th order can be seen. However, this cannot be directly related to eccentricities based on the simulation results. Since real machines are under investigation, not all tolerances are known. It can be assumed that the deviations in the 2nd and 4th order are due to other tolerances. Likewise, no further side orders caused by eccentricities are observed in the measurement as in the case of the air gap forces.

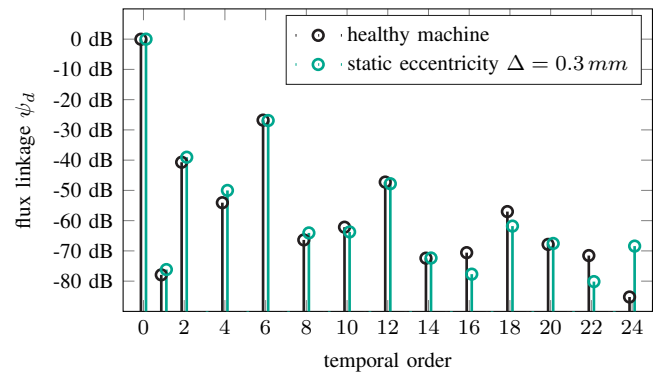


Fig. 16. Harmonic content of d-axis flux linkage under load condition

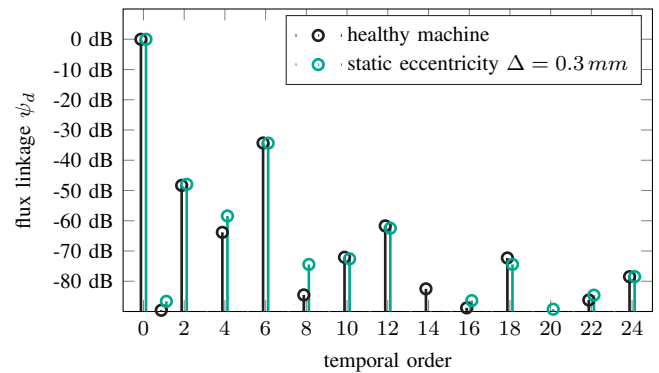


Fig. 17. Harmonic content of q-axis flux linkage under load condition

VI. CONCLUSION

The objective of this paper was to investigate the effects of eccentricities on electrical quantities. For this purpose, an FEA was first carried out. Here it was shown that the radial force density in the air gap is significantly affected by the eccentricities. Side orders of the form $\nu \pm 1$ arise in the force density, which can excite the machine to further oscillations, which leads to a changed noise behavior.

However, if the measured electrical quantities are considered, in this case the flux linkages, it was found that these are only slightly influenced by the eccentricities. The occurrence of further side orders, as in the case of the air gap forces, could not be demonstrated. This is mainly due to the fact that the machine under investigation has a symmetrical structure. Each coil group has another coil group opposite it, offset by 180° , so that the influences cancel each other out. Thus, there are no significant differences in the measured quantities at the machine terminals. Small differences exist only in the 18th order, here both forms of the eccentricities lead to a slight decrease in the amplitudes. Whether these differences are sufficient for a clear detection of eccentricities has to be shown in investigations for further operating points.

For validation, the results obtained in FEA were validated experimentally. For this purpose, a machine with static eccentricity and a machine without eccentricity were measured. Similar tendencies were found here as in the FEA. Again, no further side orders were detected. Also small differences in the 18th order could be found, which can be attributed to eccentricities based on the FEA. However, the differences in the other orders are not significant. Since these are real machines, it must be assumed that the small differences between the machines are caused by other, unknown tolerances or by the tolerance of the measurement chain.

To reliably detect eccentricities in the flux linkages, further measurements are necessary. One possibility would be to integrate two measuring coils at an offset of 90° . This would allow the position and type of eccentricity to be determined precisely. Another possibility is to measure the machine in the non-connected state. In this way, the flux linkage can be determined individually for each coil group.

REFERENCES

- [1] A. Langheck, D. Krahe, P. Breining, D. Stretz, T. Rittgerott, J. Kolb, and M. Doppelbauer, "NVH optimization in PMSM through harmonic current injection with optimum current trajectory," *Elektromechanische Antriebssysteme (VDE Verlag GmbH)*, pp. 240–247, Nov. 2021.
- [2] J.-B. Dupont and V. Lanfranchi, "Noise radiated by a permanent magnet synchronous motor: Simulation methodology and influence of motor defects," *International Conference on Electrical Machines (ICEM)*, Berlin, Germany, pp. 1321–1327, 2014.
- [3] Z. Q. Zhu, L. J. Wu, and M. L. Mohd Jamil, "Distortion of back-EMF and torque of PM brushless machines due to eccentricity," *IEEE Transactions on Magnetics*, vol. 48, no. 8, pp. 4927–4936, Aug. 2013.
- [4] M. Fischer and J. Roth-Stielow, "Analysis of the influence of static and dynamic eccentricity on back EMF of a permanent magnet synchronous motor," *Innovative Small Drives and Micro-Motor Systems, 11th GMM/ETG-Symposium, Saarbruecken, Germany*, Sep. 2017.
- [5] B. M. Ebrahimi and J. Faiz, "Diagnosis and performance analysis of three-phase permanent magnet synchronous motors with static, dynamic and mixed eccentricity," *IET Electric Power Applications*, vol. 4, no. 1, pp. 53–66, Jan. 2010.

- [6] B. M. Ebrahimi, J. Faiz, and B. N. Araabi, "Pattern identification for eccentricity fault diagnosis in permanent magnet synchronous motors using stator current monitoring," *IET Electric Power Applications*, vol. 4, no. 6, pp. 418–430, Jul. 2010.
- [7] B. M. Ebrahimi, M. J. Roshtkhari, J. Faiz, and S. V. Khatami, "Advanced eccentricity fault recognition in permanent magnet synchronous motors using stator current signature analysis," *IEEE Transactions on Industrial Electronics*, vol. 61, no. 4, pp. 2041–2052, Apr. 2014.
- [8] C. Bruzzese, "Diagnosis of eccentric rotor in synchronous machines by analysis of split-phase currents; part ii: Experimental analysis," *IEEE Transactions on Industrial Electronics*, vol. 61, no. 8, pp. 4206–4216, Aug. 2014.
- [9] J. Hong, S. B. Lee, C. Kral, and A. Haumer, "Detection of airgap eccentricity for permanent magnet synchronous motors based on the d-axis inductance," *IEEE Transactions on Power Electronics*, vol. 27, no. 5, pp. 2605–2612, May 2012.
- [10] J. Hong, D. Hyun, T. J. Kang, S. B. Lee, C. Kral, and A. Haumer, "Detection and classification of rotor demagnetization and eccentricity faults for pm synchronous motors," *IEEE Transactions on Industrial Applications*, vol. 48, no. 3, pp. 923–932, May/Jun. 2012.
- [11] J. Zhang, W. Jiang, Z. Zhang, and Z. Zhang, "Study on electromagnetic force interior permanent magnet synchronous machine with distributed windings," *IECON - 43rd Annual Conference of the IEEE Industrial Electronics Society, Beijing, China*, pp. 2190–2195, Nov. 2017.
- [12] J. R. Hendershot and T. J. E. Miller, *Design of brushless permanent-magnet machines*. Venice, Florida: Motor Design Books, 2010.
- [13] J. Richter and M. Doppelbauer, "Improving dynamics of repetitive control based current harmonic mitigation in inverter-fed permanent magnet synchronous machines with nonlinear magnetics," *8th International Conference on Power Electronics, Machines and Drives (PEMD)*, Glasgow, UK, Apr. 2016.

VII. BIOGRAPHIES

Dominik Krahe was born in Karlsruhe, Germany. He received the bachelor's and master's degree in mechanical engineering from the Karlsruhe Institute of Technology in 2014 and 2017, respectively. He is currently working towards the Ph.D. degree in electrical engineering and information technologies with the Karlsruhe Institute of Technology. His research interests include modelling, parameter identification and control of permanent magnet synchronous machines as well as the determination of NVH behavior of electrical machines due to tolerances.

Johannes Kolb was born in Pforzheim, Germany in 1982. He received his Dipl.-Ing. degree in electrical engineering from the University of Karlsruhe in 2007. From 2007 to 2013 he has been with the Institute of Electrical Engineering at the Karlsruhe Institute of Technology as research associate in the field of power electronics, where he received his Dr.-Ing. in 2013. Since then he is leading a research team in the field of electric drives and power electronics at the SHARE at KIT - a cooperation between Schaeffler Technologies AG & Co. KG and KIT.

Martin Doppelbauer was born in Altenhundem in Germany on August 26, 1965. He graduated the Technical University in Dortmund, where he received his doctorate degree in 1995 on an analytical field harmonic calculation method of AC-commutator machines. From 1995 until 2010 Martin Doppelbauer worked at Danfoss Bauer in Esslingen and at SEW Eurodrive in Bruchsal, Germany in the field of industrial electric motor development. Since 2011 Prof. Doppelbauer holds the chair of hybrid and electric vehicles with the Karlsruhe Institute of Technology (KIT). His research interest is the electrical drive train of vehicles with a particular focus on electric machines with high power density. Prof. Doppelbauer is also active in the field of standardization and currently the chairman of the Technical Committee 2 (Rotating Machinery) of the International Electrotechnical Commission (IEC) in Geneva.